Astron. Astrophys. 253, 525–536 (1992)

ASTRONOMY AND ASTROPHYSICS

Photodissociation of H_2 and the H/H_2 transition in interstellar clouds

H. Abgrall[1], J. Le Bourlot[1], G. Pineau des Forêts[1], E. Roueff[1], D.R. Flower[2], and L. Heck[2]

[1]DAEC and URA 173 du CNRS, Observatoire de Meudon, F-92195 Meudon Cedex, France
[2]Physics Dept., University of Durham, Durham DH1 3LE, UK

Received March 29, accepted May 13, 1991

Abstract. We present new data relating to the photodissociation of H_2 through absorption of ultraviolet radiation and spontaneous radiative dissociation, taking the dependence on the rotational quantum number explicitly into account. Our first application of these results is to determining the structure of the atomic to molecular hydrogen transition zone in a static cloud in equilibrium. Comparison is made with the approximate method of radiative transfer introduced by Federman et al. (1979). The validity of the assumption of equilibrium is discussed.

Key words: atomic and molecular processes – interstellar medium: extinction – interstellar medium: molecules

1. Introduction

As Stecher & Williams (1967) recognized, the photodissociation of interstellar molecular hydrogen takes place through a particular mechanism: ultraviolet absorption in the discrete lines of the Lyman ($B\ ^1\Sigma_u^+ - X\ ^1\Sigma_g^+$) and Werner ($C\ ^1\Pi_u - X\ ^1\Sigma_g^+$) band systems is followed by spontaneous emission towards the vibrational continuum of the ground electronic state. This continuous emission has been identified in laboratory spectra by Dalgarno et al. (1970) and detected recently in diffuse interstellar regions in a rocket observation by Martin et al. (1990). Stephens & Dalgarno (1972) (hereafter SD) calculated the radiative lifetimes and the fraction of radiative decay that leads to dissociation of the B and C states but neglected all rotational effects. Schmoranzer et al. (1990) were able to select specific rotationally excited levels of the B and C states using monochromatized synchrotron radiation. They studied the continuous fluorescence of H_2 both experimentally and theoretically and showed how the rotation of the molecule modifies this fluorescence. First, the centrifugal barrier shifts the positions of the fluorescence maxima; second, rotational (non-adiabatic) coupling between B and C, which gives rise to the Λ-doubling in the C state, induces intensity perturbations in the fluorescence spectrum when rovibrational states belonging to B and C become very close. These intensity perturbations have been discussed by Abgrall et al. (1987) in the context of the discrete emission spectrum of the Lyman and Werner band systems of the vacuum ultraviolet spectrum of H_2. In the present paper we extend calculations to the continuous fluorescence of H_2 and give in Sect. 2 the radiative lifetimes and dissociation fractions of a set of rovibrationally excited states. In Sect. 3 we present the first astrophysical application of these results to the study of the evolution of the H/H_2 density ratio at the edge of an interstellar cloud, where the degree of penetration of the ultraviolet interstellar radiation field depends critically on the process of photodissociation of H_2.

Send offprint requests to: E. Roueff

2. Theory

According to the definition of Brown et al. (1975), rovibronic states can be classified by their total parity. Rovibrational states belonging to the X and B electronic states of H_2 are all e-type, whereas those belonging to the C state are split by the so-called Λ-doubling into e and f levels. The e parity levels belong to Π^+ and f parity levels belong to Π^-. Fluorescence in the Lyman band system of H_2 connects levels of e parity, so only P and R transitions ($\Delta J = J' - J'' = -1, +1$, respectively) can occur. On the other hand, in the Werner band system, P, Q and R transitions ($\Delta J = -1, 0, +1$) are possible: an e–f transition occurs if $\Delta J = 0$, and e–e if $\Delta J = \pm 1$ (see Fig. 1). The net effect is to preserve the para or ortho character of H_2: absorption in a P or R transition can lead only to a P or R radiative decay, and a Q absorption can be followed only by a Q emission.

Abgrall & Roueff (1989) have systematically calculated the discrete emission spectrum of H_2 in the Lyman and Werner band system by including the rotational effects mentioned above. The three electronic dipole matrix elements which determine the emission transition probabilities (or oscillator strengths) of each branch may be written as

$$M^P = (J'+1)^{1/2}\langle f_{Bv'J'}|M_{BX}|f_{Xv''J''}\rangle + J'^{1/2}\langle f_{C^+v'J'}|M_{CX}|f_{Xv''J''}\rangle,$$

$$M^Q = \langle f_{C^-v'J'}|M_{CX}|f_{Xv''J''}\rangle,$$

$$M^R = J'^{1/2}\langle f_{Bv'J'}|M_{BX}|f_{Xv''J''}\rangle - (J'+1)^{1/2}\langle f_{C^+v'J'}|M_{CX}|f_{Xv''J''}\rangle,$$

where M_{BX} and M_{CX} are the electronic transition moments connecting the B and X, or C and X electronic states, respectively, and $f_{Xv''J''}$ is the ground rovibrational nuclear wave function (a solution of the one-dimensional Schrödinger radial equation).

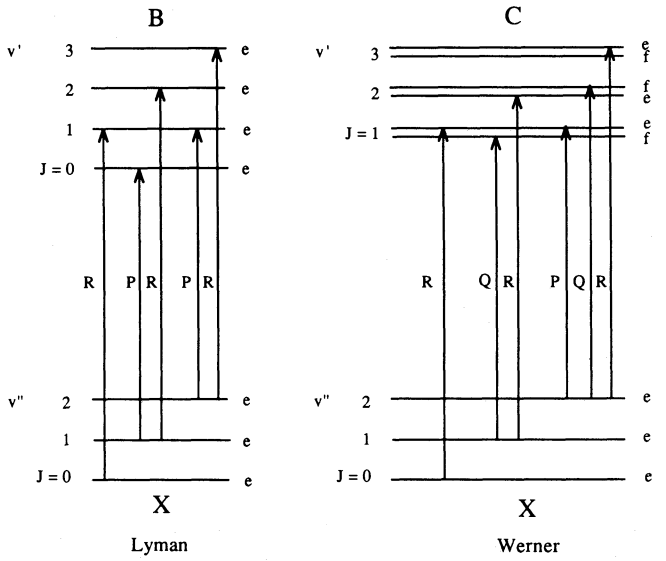

Fig. 1. Examples of allowed transitions in the H_2 Lyman and Werner bands

$f_{Bv'J'}$, $f_{C^+v'J'}$ and $f_{C^-v'J'}$ are the corresponding wave functions for the excited states; we note that the solutions for the first two are coupled by the nuclear rotation as calculated by Ford (1975) and Julienne (1973). When dissociation occurs, the final state belongs to the continuum of X $^1\Sigma_g^+$. The radial wave function is then labelled by J'' and E'', the energy above the dissociation limit of H(1s)+H(1s). We use energy-normalized wave functions which have the following asymptotic form:

$$f_{E''J''}(R) \underset{R\to\infty}{=} \sqrt{\frac{2\mu}{\pi\hbar^2 k''}} \sin\left(k''R - \frac{\pi J''}{2} + \delta_{J''}\right),$$

where $k''=\sqrt{2\mu E''}/\hbar$ is the corresponding wave number.

The emission probability to the continuum per unit energy interval is then given by

$$A_{v'J',E''J''}\,\mathrm{d}E'' = \frac{4}{3\hbar^4 c^3\,(2J'+1)}\,(E_{v'J'}-E_{v''J''})|M^\alpha|^2\,\mathrm{d}E'',$$

with M^α calculated from the functions $f_{E''J''}(R)$. The total probability of emission in a transition from a given upper state $v'J'$ to the continuum of the ground state is (in s^{-1})

$$A^{\mathrm{cont}}_{v'J'} = \int_0^\infty A_{v'J',E''J''}\,\mathrm{d}E''.$$

We have calculated these integrals for each rovibrational level using the same potentials and numerical methods as Abgrall & Roueff (1989).

The total decay probability, $A^{\mathrm{t}}_{v'J'} = A^{\mathrm{bound}}_{v'J'} + A^{\mathrm{cont}}_{v'J'}$, where $A^{\mathrm{bound}}_{v'J'} = \sum_{v''J''} A_{v'J',v''J''}$ is the total probability of a transition from an upper level $v'J'$ into any bound level of the ground state, and the dissociation probability $d_{v'J'} = A^{\mathrm{cont}}_{v'J'}/A^{\mathrm{t}}_{v'J'}$ for B, C^+ and C^- states, respectively, are given in Tables 1, 2 and 3 together with the results of SD for the dissociation probabilities calculated only for $J=0$.

The vibrational levels which can be reached by photons of energies smaller than 13.6 eV and rotational levels with $J \leq 10$ are given. Additional results can be provided upon request. We note that the total decay probabilities do not vary much with J', and their values are close to those given by SD. The dissociation probabilities of the B state are also very close to the results of SD when the values are not exceedingly small ($d > 10^{-5}$). However, the probabilities vary with J. Furthermore, there are significant differences between C^+ and C^- dissociation probabilities, which may differ by several orders of magnitudes within a single Λ-doublet. In that case, the SD values apply only to C^-.

Table 1. Inverse of the lifetimes and dissociation fractions (DF) of the B state of H_2

v	J	A (tot) (s^{-1})	DF		v	J	A (tot) (s^{-1})	DF	
			This work	SD				This work	SD
0	0	1.866 (9)	1.580 (−6)	3.015 (−9)	1	6	1.697 (9)	1.096 (−6)	
0	1	1.864 (9)	1.486 (−6)		1	7	1.683 (9)	1.929 (−6)	
0	2	1.859 (9)	1.470 (−6)		1	8	1.666 (9)	2.110 (−6)	
0	3	1.852 (9)	1.366 (−6)		1	9	1.648 (9)	4.023 (−6)	
0	4	1.843 (9)	1.349 (−6)		1	10	1.628 (9)	1.009 (−5)	
0	5	1.831 (9)	1.414 (−6)						
0	6	1.817 (9)	1.250 (−6)		2	0	1.632 (9)	1.183 (−5)	1.346 (−5)
0	7	1.801 (9)	1.428 (−6)		2	1	1.630 (9)	1.198 (−5)	
0	8	1.782 (9)	1.320 (−6)		2	2	1.626 (9)	1.225 (−5)	
0	9	1.761 (9)	1.584 (−6)		2	3	1.621 (9)	1.232 (−5)	
0	10	1.738 (9)	1.536 (−6)		2	4	1.613 (9)	1.198 (−5)	
1	0	1.741 (9)	3.250 (−7)	6.579 (−8)	2	5	1.604 (9)	1.270 (−5)	
1	1	1.739 (9)	3.478 (−7)		2	6	1.592 (9)	1.791 (−5)	
1	2	1.735 (9)	3.630 (−7)		2	7	1.580 (9)	6.458 (−5)	
1	3	1.728 (9)	4.171 (−7)		2	8	1.565 (9)	9.039 (−5)	
1	4	1.720 (9)	5.344 (−7)		2	9	1.549 (9)	1.641 (−4)	
1	5	1.710 (9)	7.162 (−7)		2	10	1.531 (9)	2.001 (−4)	

Table 1 (Continued)

v	J	A (tot) (s^{-1})	DF		v	J	A (tot) (s^{-1})	DF	
			This work	SD				This work	SD
3	0	1.536 (9)	1.308 (−4)	1.346 (−5)	7	9	1.192 (9)	4.130 (−1)	
3	1	1.534 (9)	1.506 (−4)		7	10	1.159 (9)	4.375 (−1)	
3	2	1.531 (9)	1.951 (−4)						
3	3	1.525 (9)	2.759 (−4)		8	0	1.178 (9)	3.016 (−1)	2.909 (−1)
3	4	1.519 (9)	4.211 (−4)		8	1	1.177 (9)	3.121 (−1)	
3	5	1.510 (9)	5.073 (−4)		8	2	1.175 (9)	3.331 (−1)	
3	6	1.500 (9)	6.383 (−4)		8	3	1.172 (9)	3.633 (−1)	
3	7	1.488 (9)	6.776 (−4)		8	4	1.167 (9)	3.962 (−1)	
3	8	1.475 (9)	8.807 (−4)		8	5	1.162 (9)	4.002 (−1)	
3	9	1.461 (9)	1.396 (−3)		8	6	1.166 (9)	2.381 (−1)	
3	10	1.444 (9)	3.646 (−3)		8	7	1.149 (9)	4.366 (−1)	
					8	8	1.137 (9)	4.318 (−1)	
4	0	1.450 (9)	1.325 (−3)	1.485 (−3)	8	9	1.129 (9)	4.449 (−1)	
4	1	1.449 (9)	1.282 (−3)		8	10	1.115 (9)	4.438 (−1)	
4	2	1.445 (9)	1.222 (−3)						
4	3	1.441 (9)	1.255 (−3)		9	0	1.123 (9)	4.133 (−1)	4.152 (−1)
4	4	1.434 (9)	1.885 (−3)		9	1	1.122 (9)	4.125 (−1)	
4	5	1.427 (9)	2.767 (−3)		9	2	1.120 (9)	4.122 (−1)	
4	6	1.417 (9)	4.626 (−3)		9	3	1.117 (9)	4.153 (−1)	
4	7	1.407 (9)	9.486 (−3)		9	4	1.112 (9)	4.266 (−1)	
4	8	1.395 (9)	9.724 (−3)		9	5	1.107 (9)	4.250 (−1)	
4	9	1.382 (9)	1.546 (−2)		9	6	1.101 (9)	4.273 (−1)	
4	10	1.365 (9)	2.238 (−2)		9	7	1.095 (9)	4.328 (−1)	
					9	8	1.086 (9)	4.240 (−1)	
5	0	1.373 (9)	1.779 (−2)	1.706 (−2)	9	9	1.080 (9)	4.307 (−1)	
5	1	1.371 (9)	1.861 (−2)		9	10	1.085 (9)	2.881 (−1)	
5	2	1.368 (9)	2.009 (−2)						
5	3	1.364 (9)	2.184 (−2)		10	0	1.073 (9)	4.103 (−1)	4.103 (−1)
5	4	1.358 (9)	2.296 (−2)		10	1	1.072 (9)	4.100 (−1)	
5	5	1.351 (9)	2.253 (−2)		10	2	1.070 (9)	4.096 (−1)	
5	6	1.342 (9)	2.333 (−2)		10	3	1.068 (9)	4.097 (−1)	
5	7	1.334 (9)	4.090 (−2)		10	4	1.068 (9)	4.028 (−1)	
5	8	1.322 (9)	4.885 (−2)		10	5	1.088 (9)	2.511 (−1)	
5	9	1.311 (9)	7.136 (−2)		10	6	1.052 (9)	4.077 (−1)	
5	10	1.296 (9)	8.563 (−2)		10	7	1.050 (9)	4.726 (−1)	
					10	8	1.037 (9)	4.677 (−1)	
6	0	1.302 (9)	3.123 (−2)	3.089 (−2)	10	9	1.033 (9)	5.142 (−1)	
6	1	1.301 (9)	3.331 (−2)		10	10	1.017 (9)	5.150 (−1)	
6	2	1.298 (9)	3.895 (−2)						
6	3	1.294 (9)	5.191 (−2)		11	0	1.025 (9)	4.063 (−1)	4.074 (−1)
6	4	1.289 (9)	8.243 (−2)		11	1	1.024 (9)	4.071 (−1)	
6	5	1.282 (9)	1.008 (−1)		11	2	1.022 (9)	4.112 (−1)	
6	6	1.274 (9)	1.308 (−1)		11	3	1.020 (9)	4.259 (−1)	
6	7	1.265 (9)	1.390 (−1)		11	4	1.016 (9)	4.753 (−1)	
6	8	1.255 (9)	1.446 (−1)		11	5	1.012 (9)	4.857 (−1)	
6	9	1.245 (9)	1.721 (−1)		11	6	1.006 (9)	5.206 (−1)	
6	10	1.207 (9)	2.815 (−1)		11	7	1.002 (9)	5.232 (−1)	
					11	8	9.966 (8)	5.149 (−1)	
7	0	1.237 (9)	2.074 (−1)	2.111 (−1)	11	9	1.034 (9)	3.638 (−1)	
7	1	1.236 (9)	2.054 (−1)		11	10	9.771 (8)	5.091 (−1)	
7	2	1.234 (9)	2.004 (−1)						
7	3	1.230 (9)	1.920 (−1)		12	0	9.817 (8)	5.233 (−1)	5.229 (−1)
7	4	1.225 (9)	1.889 (−1)		12	1	9.814 (8)	5.199 (−1)	
7	5	1.219 (9)	1.926 (−1)		12	2	9.824 (8)	5.084 (−1)	
7	6	1.211 (9)	2.139 (−1)		12	3	1.002 (9)	4.320 (−1)	
7	7	1.211 (9)	3.299 (−1)		12	4	9.941 (8)	4.339 (−1)	
7	8	1.194 (9)	3.261 (−1)		12	5	9.716 (8)	5.024 (−1)	

Table 1 (Continued)

v	J	A (tot) (s^{-1})	DF		v	J	A (tot) (s^{-1})	DF	
			This work	SD				This work	SD
12	6	9.640 (8)	5.160 (−1)		17	3	8.023 (8)	6.028 (−1)	
12	7	9.587 (8)	5.239 (−1)		17	4	8.021 (8)	6.005 (−1)	
12	8	9.509 (8)	5.194 (−1)		17	5	8.068 (8)	5.809 (−1)	
12	9	9.457 (8)	5.298 (−1)		17	6	8.557 (8)	4.552 (−1)	
12	10	9.317 (8)	5.412 (−1)		17	7	8.298 (8)	4.910 (−1)	
13	0	9.410 (8)	5.111 (−1)	5.109 (−1)	17	8	7.898 (8)	5.845 (−1)	
13	1	9.402 (8)	5.097 (−1)		17	9	7.806 (8)	6.048 (−1)	
13	2	9.386 (8)	5.072 (−1)		17	10	7.719 (8)	6.113 (−1)	
13	3	9.365 (8)	5.062 (−1)		18	0	7.755 (8)	6.111 (−1)	6.077 (−1)
13	4	9.333 (8)	5.227 (−1)		18	1	7.753 (8)	6.090 (−1)	
13	5	9.300 (8)	5.183 (−1)		18	2	7.747 (8)	6.057 (−1)	
13	6	9.263 (8)	5.298 (−1)		18	3	7.734 (8)	6.011 (−1)	
13	7	9.275 (8)	5.326 (−1)		18	4	7.712 (8)	6.111 (−1)	
13	8	9.598 (8)	4.199 (−1)		18	5	7.687 (8)	6.070 (−1)	
13	9	9.175 (8)	5.121 (−1)		18	6	7.657 (8)	6.173 (−1)	
13	10	8.988 (8)	5.567 (−1)		18	7	7.635 (8)	6.151 (−1)	
14	0	9.031 (8)	5.397 (−1)	5.424 (−1)	18	8	7.621 (8)	6.071 (−1)	
14	1	9.704 (8)	3.481 (−1)		18	9	7.754 (8)	5.658 (−1)	
14	2	9.269 (8)	4.497 (−1)		18	10	8.625 (8)	3.432 (−1)	
14	3	9.065 (8)	4.984 (−1)		19	0	7.488 (8)	6.364 (−1)	6.339 (−1)
14	4	8.988 (8)	5.315 (−1)		19	1	7.487 (8)	6.348 (−1)	
14	5	8.935 (8)	5.358 (−1)		19	2	7.489 (8)	6.304 (−1)	
14	6	8.882 (8)	5.555 (−1)		19	3	7.504 (8)	6.186 (−1)	
14	7	8.829 (8)	5.602 (−1)		19	4	7.594 (8)	5.944 (−1)	
14	8	8.774 (8)	5.636 (−1)		19	5	8.345 (8)	4.161 (−1)	
14	9	8.721 (8)	5.644 (−1)		19	6	7.845 (8)	5.050 (−1)	
14	10	8.665 (8)	5.650 (−1)		19	7	7.447 (8)	5.986 (−1)	
15	0	8.678 (8)	5.603 (−1)	5.583 (−1)	19	8	7.338 (8)	6.180 (−1)	
15	1	8.672 (8)	5.596 (−1)		19	9	7.279 (8)	6.251 (−1)	
15	2	8.660 (8)	5.580 (−1)		19	10	7.222 (8)	6.325 (−1)	
15	3	8.643 (8)	5.548 (−1)		20	0	7.242 (8)	6.392 (−1)	6.374 (−1)
15	4	8.621 (8)	5.574 (−1)		20	1	7.239 (8)	6.377 (−1)	
15	5	8.605 (8)	5.521 (−1)		20	2	7.234 (8)	6.350 (−1)	
15	6	8.621 (8)	5.432 (−1)		20	3	7.224 (8)	6.304 (−1)	
15	7	9.018 (8)	4.498 (−1)		20	4	7.208 (8)	6.310 (−1)	
15	8	8.700 (8)	4.931 (−1)		20	5	7.190 (8)	6.262 (−1)	
15	9	8.424 (8)	5.778 (−1)		20	6	7.174 (8)	6.272 (−1)	
15	10	8.313 (8)	5.884 (−1)		20	7	7.186 (8)	6.241 (−1)	
16	0	8.347 (8)	5.559 (−1)	5.543 (−1)	20	8	7.286 (8)	5.904 (−1)	
16	1	8.354 (8)	5.507 (−1)		20	9	8.579 (8)	3.205 (−1)	
16	2	8.349 (8)	5.461 (−1)		20	10	7.198 (8)	5.889 (−1)	
16	3	8.331 (8)	5.442 (−1)		21	0	7.016 (8)	6.435 (−1)	6.426 (−1)
16	4	8.300 (8)	5.693 (−1)		21	1	7.024 (8)	6.394 (−1)	
16	5	8.266 (8)	5.710 (−1)		21	2	7.061 (8)	6.263 (−1)	
16	6	8.226 (8)	5.941 (−1)		21	3	7.251 (8)	5.731 (−1)	
16	7	8.186 (8)	5.966 (−1)		21	4	8.654 (8)	2.935 (−1)	
16	8	8.145 (8)	5.971 (−1)		21	5	7.343 (8)	5.399 (−1)	
16	9	8.127 (8)	5.910 (−1)		21	6	7.039 (8)	6.141 (−1)	
16	10	8.296 (8)	5.358 (−1)		21	7	6.943 (8)	6.367 (−1)	
17	0	8.043 (8)	6.062 (−1)	6.011 (−1)	21	8	6.886 (8)	6.463 (−1)	
17	1	8.038 (8)	6.064 (−1)		21	9	6.849 (8)	6.513 (−1)	
17	2	8.031 (8)	6.061 (−1)		21	10	6.839 (8)	6.503 (−1)	

Table 1 (Continued)

v	J	A (tot) (s^{-1})	DF		v	J	A (tot) (s^{-1})	DF	
			This work	SD				This work	SD
22	0	6.806 (8)	6.529 (−1)	6.512 (−1)	22	6	6.787 (8)	6.433 (−1)	
22	1	6.803 (8)	6.525 (−1)		22	7	6.893 (8)	6.228 (−1)	
22	2	6.800 (8)	6.521 (−1)		22	8	7.721 (8)	4.390 (−1)	
22	3	6.793 (8)	6.511 (−1)		22	9	7.105 (8)	5.480 (−1)	
22	4	6.784 (8)	6.509 (−1)		22	10	6.672 (8)	6.519 (−1)	
22	5	6.777 (8)	6.484 (−1)						

Table 2. Inverse of the lifetimes and dissociation fractions (DF) of the C^+ state of H_2

		A (tot) (s^{-1})	DF This work			A (tot) (s^{-1})	DF This work
v	J			v	J		
0	1	1.180 (9)	1.353 (−4)	4	1	1.103 (9)	2.873 (−3)
0	2	1.179 (9)	3.680 (−4)	4	2	1.101 (9)	5.284 (−3)
0	3	1.178 (9)	7.293 (−4)	4	3	1.099 (9)	6.924 (−3)
0	4	1.176 (9)	1.545 (−3)	4	4	1.095 (9)	9.907 (−3)
0	5	1.172 (9)	5.389 (−3)	4	5	1.085 (9)	1.978 (−2)
0	6	1.158 (9)	1.763 (−1)	4	6	1.030 (9)	9.695 (−2)
0	7	1.168 (9)	7.939 (−3)	4	7	1.048 (9)	7.898 (−2)
0	8	1.163 (9)	3.272 (−3)	4	8	1.075 (9)	2.656 (−2)
0	9	1.157 (9)	5.397 (−3)	4	9	1.058 (9)	3.984 (−2)
0	10	1.123 (9)	1.641 (−1)	4	10	9.603 (8)	1.920 (−1)
1	1	1.159 (9)	3.891 (−4)	5	1	1.090 (9)	1.334 (−3)
1	2	1.158 (9)	1.278 (−3)	5	2	1.087 (9)	3.713 (−3)
1	3	1.156 (9)	3.537 (−3)	5	3	1.082 (9)	8.022 (−3)
1	4	1.150 (9)	1.529 (−2)	5	4	1.069 (9)	2.219 (−2)
1	5	1.122 (9)	1.513 (−1)	5	5	9.886 (8)	1.266 (−1)
1	6	1.148 (9)	1.449 (−2)	5	6	1.031 (9)	7.485 (−2)
1	7	1.146 (9)	7.962 (−3)	5	7	1.061 (9)	2.881 (−2)
1	8	1.139 (9)	1.153 (−2)	5	8	1.049 (9)	3.622 (−2)
1	9	1.089 (9)	1.335 (−1)	5	9	9.124 (8)	2.111 (−1)
1	10	1.131 (9)	1.708 (−2)	5	10	1.038 (9)	4.715 (−2)
2	1	1.138 (9)	1.599 (−3)	6	1	1.077 (9)	2.584 (−3)
2	2	1.135 (9)	8.201 (−3)	6	2	1.071 (9)	8.265 (−3)
2	3	1.111 (9)	6.491 (−2)	6	3	1.049 (9)	3.119 (−2)
2	4	1.113 (9)	7.190 (−2)	6	4	9.043 (8)	2.213 (−1)
2	5	1.129 (9)	1.668 (−2)	6	5	1.030 (9)	5.545 (−2)
2	6	1.127 (9)	1.048 (−2)	6	6	1.051 (9)	2.690 (−2)
2	7	1.120 (9)	1.564 (−2)	6	7	1.042 (9)	3.228 (−2)
2	8	1.075 (9)	9.492 (−2)	6	8	9.527 (8)	1.289 (−1)
2	9	1.107 (9)	3.862 (−2)	6	9	1.006 (9)	7.955 (−2)
2	10	1.108 (9)	1.650 (−2)	6	10	1.027 (9)	5.142 (−2)
3	1	1.053 (9)	1.396 (−1)	7	1	1.060 (9)	1.166 (−2)
3	2	1.094 (9)	5.735 (−2)	7	2	9.853 (8)	9.087 (−2)
3	3	1.110 (9)	2.020 (−2)	7	3	9.719 (8)	1.104 (−1)
3	4	1.112 (9)	1.254 (−2)	7	4	1.037 (9)	3.966 (−2)
3	5	1.110 (9)	1.145 (−2)	7	5	1.046 (9)	2.981 (−2)
3	6	1.102 (9)	1.827 (−2)	7	6	1.038 (9)	3.875 (−2)
3	7	1.056 (9)	8.930 (−2)	7	7	9.802 (8)	1.011 (−1)
3	8	1.076 (9)	6.265 (−2)	7	8	9.539 (8)	1.502 (−1)
3	9	1.092 (9)	2.201 (−2)	7	9	1.022 (9)	8.141 (−2)
3	10	1.066 (9)	4.689 (−2)	7	10	9.784 (8)	1.266 (−1)

Table 3. Inverse of the lifetimes and dissociation fractions (DF) of the C^- state of H_2

		A (tot) (s^{-1})	DF				A (tot) (s^{-1})	DF	
			This work	SD				This work	SD
v	J				v	J			
0	1	1.180 (9)	1.218 (−9)	1.208 (−11)	4	1	1.105 (9)	2.277 (−6)	2.041 (−6)
0	2	1.179 (9)	1.185 (−9)		4	2	1.104 (9)	2.442 (−6)	
0	3	1.177 (9)	1.047 (−9)		4	3	1.103 (9)	2.645 (−6)	
0	4	1.175 (9)	1.159 (−9)		4	4	1.101 (9)	2.802 (−6)	
0	5	1.172 (9)	1.154 (−9)		4	5	1.099 (9)	2.731 (−6)	
0	6	1.168 (9)	8.889 (−10)		4	6	1.096 (9)	2.175 (−6)	
0	7	1.164 (9)	8.476 (−10)		4	7	1.093 (9)	1.964 (−6)	
0	8	1.160 (9)	7.671 (−10)		4	8	1.090 (9)	1.048 (−5)	
0	9	1.155 (9)	7.266 (−10)		4	9	1.086 (9)	2.488 (−5)	
0	10	1.149 (9)	6.405 (−10)		4	10	1.083 (9)	5.649 (−5)	
1	1	1.159 (9)	2.197 (−10)	1.103 (−10)	5	1	1.091 (9)	8.583 (−6)	7.435 (−6)
1	2	1.158 (9)	1.809 (−10)		5	2	1.090 (9)	1.135 (−5)	
1	3	1.156 (9)	2.121 (−10)		5	3	1.089 (9)	1.829 (−5)	
1	4	1.154 (9)	1.658 (−10)		5	4	1.087 (9)	3.581 (−5)	
1	5	1.151 (9)	1.674 (−10)		5	5	1.085 (9)	8.762 (−5)	
1	6	1.148 (9)	1.624 (−10)		5	6	1.083 (9)	1.433 (−4)	
1	7	1.144 (9)	1.611 (−10)		5	7	1.080 (9)	2.300 (−4)	
1	8	1.140 (9)	2.217 (−10)		5	8	1.078 (9)	4.870 (−4)	
1	9	1.135 (9)	1.739 (−10)		5	9	1.075 (9)	4.690 (−4)	
1	10	1.130 (9)	1.083 (−10)		5	10	1.071 (9)	3.787 (−4)	
2	1	1.139 (9)	3.205 (−10)	2.404 (−9)	6	1	1.079 (9)	6.837 (−4)	6.753 (−4)
2	2	1.138 (9)	3.379 (−10)		6	2	1.078 (9)	7.478 (−4)	
2	3	1.136 (9)	3.892 (−10)		6	3	1.077 (9)	8.375 (−4)	
2	4	1.134 (9)	4.313 (−10)		6	4	1.076 (9)	9.375 (−4)	
2	5	1.132 (9)	3.946 (−10)		6	7	1.074 (9)	1.010 (−3)	
2	6	1.129 (9)	3.473 (−10)		6	6	1.072 (9)	8.666 (−4)	
2	7	1.125 (9)	8.260 (−10)		6	7	1.070 (9)	6.897 (−4)	
2	8	1.121 (9)	9.876 (−9)		6	8	1.068 (9)	1.668 (−3)	
2	9	1.117 (9)	2.528 (−8)		6	9	1.065 (9)	3.466 (−3)	
2	10	1.112 (9)	6.063 (−8)		6	10	1.063 (9)	7.449 (−3)	
3	1	1.121 (9)	1.838 (−8)	2.031 (−8)	7	1	1.070 (9)	1.396 (−3)	1.454 (−3)
3	2	1.120 (9)	2.667 (−8)		7	2	1.070 (9)	1.495 (−3)	
3	3	1.119 (9)	4.508 (−8)		7	3	1.069 (9)	1.887 (−3)	
3	4	1.117 (9)	8.665 (−8)		7	4	1.068 (9)	3.170 (−3)	
3	5	1.114 (9)	1.966 (−7)		7	5	1.067 (9)	7.680 (−3)	
3	6	1.111 (9)	3.148 (−7)		7	6	1.065 (9)	1.223 (−2)	
3	7	1.108 (9)	4.906 (−7)		7	7	1.064 (9)	1.928 (−2)	
3	8	1.105 (9)	9.328 (−7)		7	8	1.063 (9)	4.162 (−2)	
3	9	1.101 (9)	8.616 (−7)		7	9	1.060 (9)	3.858 (−2)	
3	10	1.096 (9)	6.340 (−7)		7	10	1.058 (9)	3.176 (−2)	

3. Application to the H–H_2 transition region

We have used these photodissociation probabilities to study the transition from atomic to molecular hydrogen in the outer layers of a molecular cloud. The conversion of H to H_2 is controlled by two main processes:

(i) formation of H_2 on interstellar grains:
$H + H + \text{Grain} \rightarrow H_2 + \text{Grain}$.

(ii) destruction of H_2 through photodissociation:
$H_2 + h\nu \rightarrow H_2^* \rightarrow H + H + h\nu$.

Since the photodissociation of interstellar H_2 is initiated by absorption through discrete lines of the Lyman and Werner bands as mentioned above, the radiation field is quickly attenuated at the wavelengths of the absorption lines as the optical depth increases. For a given transition at a given point inside the cloud, this attenuation is mainly due to absorption from the edge of the cloud in the same line. This "self-shielding" process has been described by Federman et al. (1979) (hereafter FGK), who derived an analytical approximation to the self-shielding in a line. However, the core of the line becomes rapidly saturated, and most

of the absorption then occurs in the wings. In this case, attenuation by adjacent lines can play a non-negligible part in the shielding, so that a complete knowledge of the radiation field as a function of depth inside the cloud is needed. Absorption in the Lyman lines of atomic hydrogen have also been taken into account up to levels with $n=50$, as indicated by van Dishoeck & Black (1988).

We have used an improved version of the model of Le Bourlot (1991). A numerical treatment of the radiative transfer has been included assuming a plane parallel geometry with the radiation incident on one side. We consider only models with constant density and temperature, with an emphasis on the effects of the radiation on the abundance of H_2. In our reference model, we have adopted $n_H = n(H) + 2n(H_2) = 20\ cm^{-3}$ and $T = 80$ K. The cosmic ray ionization rate is taken equal to $10^{-17}\ s^{-1}$, the incident radiation field is from Mathis et al. (1983) for a distance of 10 kpc from the galactic centre and considered as "standard". They give the energy density and attenuation properties of grains from the Lyman cutoff to the millimeter region. The elemental abundances are assumed to be cosmic as reported in Table 4 and taken from Anders & Grevesse (1989).

The fluorescence of H_2 is treated using the cascade formalism introduced by Black & Dalgarno (1977) and developed by Viala et al. (1988), including all 15 vibrational levels of the ground state.

Table 4

	Elemental abundances from Anders & Grevesse (1989)
H	1.00
He	1.00 (−1)
C	3.62 (−4)
N	1.12 (−4)
O	8.53 (−4)

The excitation of the molecule is computed including the effects of collisions with various partners. The corresponding data are summarized in Table 5. The J-dependence which arises in the formation of H_2 on grains (we assume an ortho-to-para ratio of 3) in gas phase chemical reactions [2/3 in H_2 ($J=1$) and 1/3 in H_2 ($J=0$)] and, of course, in photodissociation is also taken into account. Our calculations include the first 15 rotational levels of H_2.

The only approximation in the radiative transfer is to neglect the source function resulting from the fluorescence process in H_2. This assumption is valid in our case since these photons are reemitted isotropically and, thus, contribute a negligible amount to the incoming radiation. Each line is described by a Voigt profile with a Doppler core, including thermal and microturbulent broadening with a velocity $b = 1\ km\ s^{-1}$. The radiation field is divided into about 300 000 equally spaced mesh points, from 91.0 to 126.0 nm, and is computed at each of about 50 grid points from the surface of the cloud to an optical depth $\tau_v = 1$. Integration of this radiation field across a line profile must usually be carried far into the wings (up to several nanometers for the strongest line) in order to allow for absorption outside the fully saturated core. A part of the calculated spectrum is shown in Fig. 2 for two optical depths inside the cloud ($\tau_v = 0.1$ and $\tau_v = 0.5$). Several points are worth mentioning:

(i) Absorption by grains leads to an overall decrease of one magnitude in the radiative energy density, from $\tau_v = 0.1$ to $\tau_v = 0.5$.

(ii) At $\tau_v = 0.1$, the absorption line system is already rich: H Lyδ at 949.743 Å is present (label a in Fig. 2), whereas all other lines belong to H_2. The weakest features arise from levels with $J \geq 2$ (e.g. X ($v''=0$, $J''=3$)→B ($v'=15$, $J'=2$), label b in Fig. 2), but some lines are already saturated (e.g. X ($v''=0$, $J''=0$)→C ($v'=3$, $J'=0$), label c in Fig. 2) and the effects of line overlap are obvious.

(iii) At $\tau_v = 0.5$, the strongest lines are completely blended and their overlapping wings extend over more than 1.5 nm. In contrast, the H Lyδ line is nearly unchanged since most of H has already been converted to H_2 in this region.

Table 5. Collisional de-excitation and reactive ortho→para rate coefficients used in the calculations. (a): Elitzur & Watson (1978), (b): Danby et al. (1986), (c): Schaeffer (1985, private communication), (d): Gerlich (1990), (e): Schofield (1967)

Collision partner	Ref.	Rate coefficient or formula used
H	(a)	Eqs. (1)–(5)
H_2	(b)	$q(J \to J-2) = 10^{-11}\ [A(J)T^{B(J)} + C(J)]\ cm^3\ s^{-1}$, $0 \leq J \leq 7$ Extrapolation for $7 < J < 15$. Coefficients A, B, C are given in Table 6.
He	(c)	$q(J \to J-2) = 10^{AA(J)\log(T)+BB(J)}\ cm^3\ s^{-1}$, $0 \leq J \leq 6$ Coefficient AA & BB from ref. (c), Extrapolated as follows for $J > 6$: $AA(J) = -3.33\ 10^{-2} J^2 + 0.531 J + 0.277$ $BB(J) = 6.39\ 10^{-2} J^2 - 1.50 J - 11.7$
H^+	(d)	$0 \leq J \leq 9$ Main contributions for $q(1 \to 0) = 2.0\ 10^{-10}$, $q(2 \to 1) = 9.6\ 10^{-10}\ cm^3\ s^{-1}$
H_3^+		Taken to be the same as for H^+ exchange.
H	(e)	$q(1 \to 0) = 8.9\ 10^{-12} \exp(-3730/T)\ cm^3\ s^{-1}$

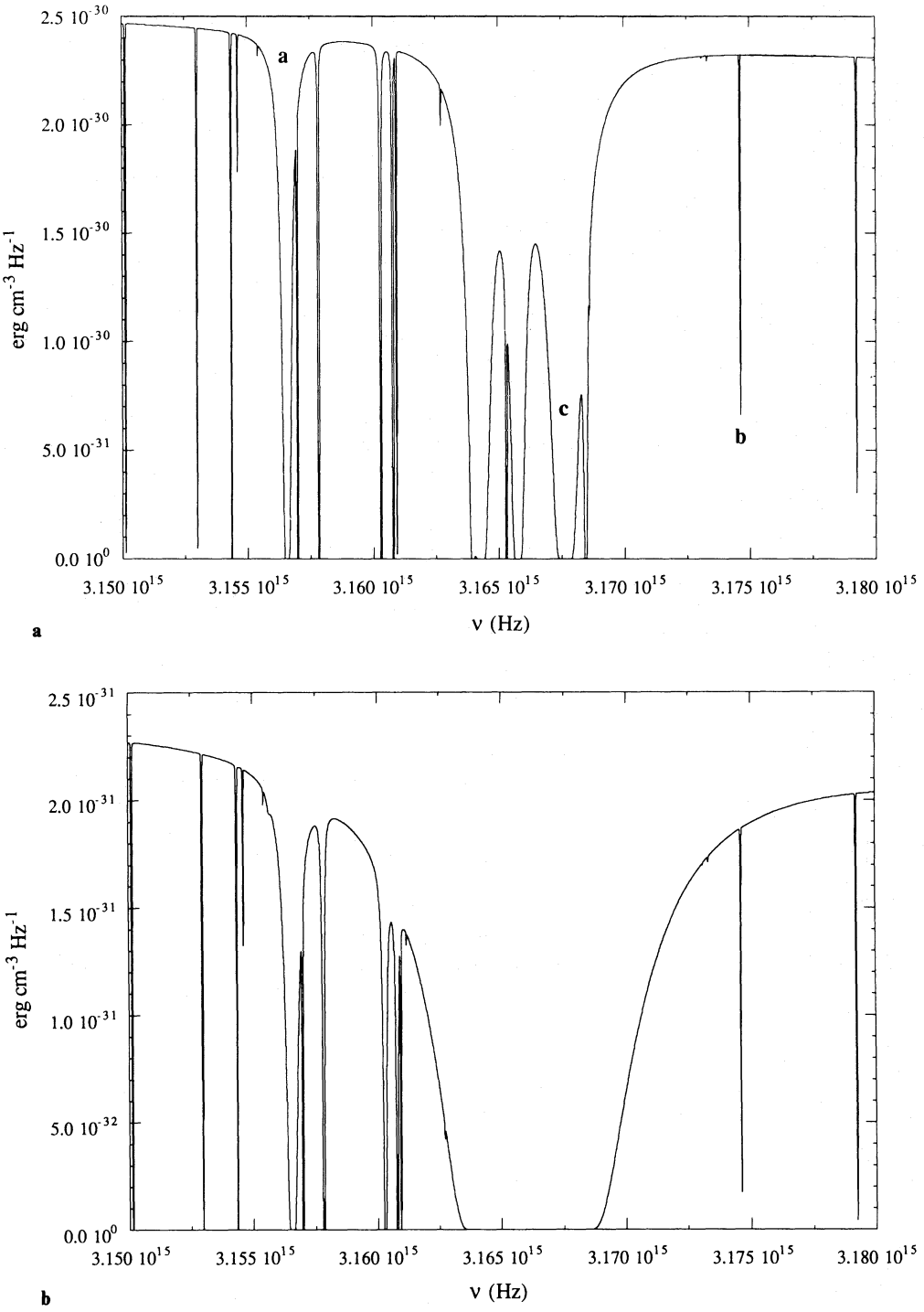

Fig. 2a and b. A section of the radiation field, as computed at **a** $\tau_v = 0.1$, and **b** $\tau_v = 0.5$

The fraction of discrete absorptions from the various initial rotational states of $v=0$ leading to dissociation of H_2 has been calculated and is of the order of 13% for the standard radiation field, a result close to the 10% estimate of Stephens & Dalgarno (1972).

The chemical network includes 60 species containing H, He, C, N and O and 473 chemical reactions. The chemistry, which does not play a primordial role in the H–H_2 transition region, is an extension of the one used by Pineau des Forêts et al. (1986) and will be published in a future paper.

In Fig. 3, we compare the results of our numerical model with the approximation of FGK. The two models differ only in the treatment of the radiative transfer. Figure 3a displays the variations of the H, H_2 and H^+ abundances as a function of the optical depth, Fig. 3b shows the photodissociation rate of H_2 as a function of the optical depth in the cloud, and Fig. 3c shows the ratio of the photodissociation rates using the two methods. At the extreme edge of the cloud, the photodissociation rate is the same for the two methods and equal to $2.36\,10^{-11}\,s^{-1}$. This value is compatible with that of $4\,10^{-11}\,s^{-1}$ of van Dishoeck (1988) since

Table 6. Coefficients $A(J)$, $B(J)$, $C(J)$ used in the second entry of Table 5

J	2	3	4	5	6	7	8
$A(J)$	3.17 (−4)	2.38 (−5)	1.94 (−6)	1.67 (−7)	1.60 (−8)	2.32 (−9)	3.06 (−10)
$B(J)$	1.165	1.512	1.831	2.113	2.376	2.575	2.760
$C(J)$	3.07 (−2)	1.12 (−2)	5.43 (−3)	1.98 (−3)	7.53 (−4)	2.77 (−4)	9.88 (−5)

J	9	10	11	12	13	14
$A(J)$	4.94 (−11)	9.16 (−12)	1.96 (−12)	4.81 (−13)	1.36 (−13)	4.42 (−14)
B(J)	2.906	3.018	3.095	3.138	3.146	3.120
C(J)	3.40 (−5)	1.13 (−5)	3.63 (−6)	1.13 (−6)	3.39 (−7)	9.84 (−8)

we consider here only half of the total background radiation field, the irradiation coming from only one side of the cloud.

The FGK approximation is seen to yield a good representation of the transition region between the atomic and molecular gas. The net effect of a full treatment of the radiative transfer is to shift the transition region somewhat further into the cloud, but this will not be observable due to the small thickness of this layer (10^{-2} magnitude). For an $A_v > 1$, FGK overestimate the photodissociation probabilities by orders of magnitude, but this does not change the abundances since reprocessing by the chemistry is much more efficient there. It is also worthwhile to note that the CPU time ratio for one complete model between the two treatments is between 8 and 10, depending upon the density structure of the cloud.

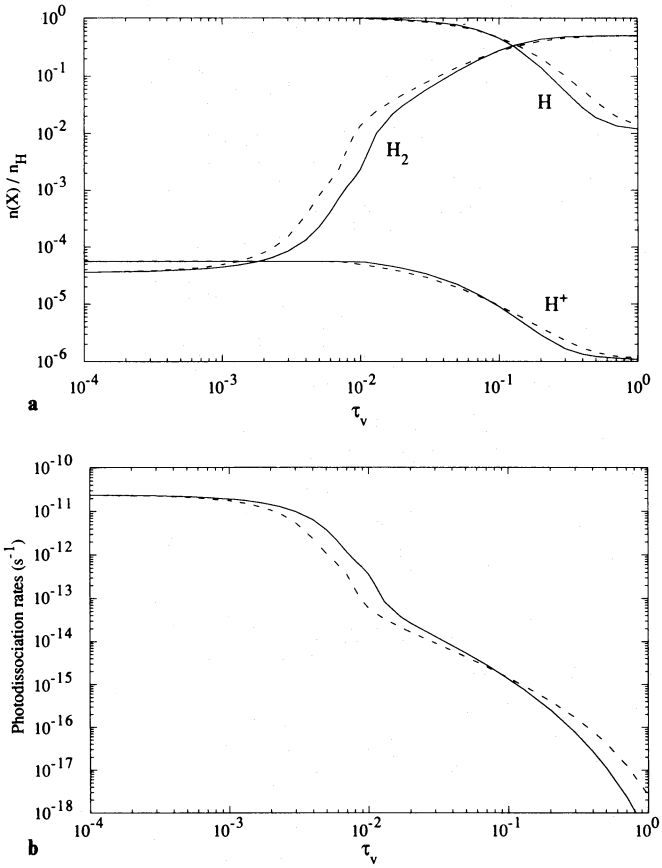

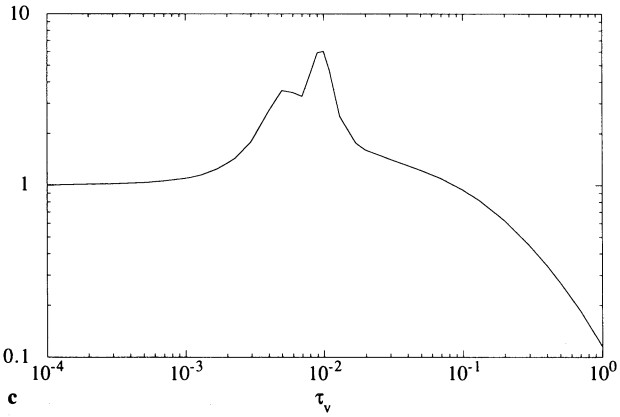

Fig. 3a–c. A comparison of **a** the relative abundances of H_2, H and H^+, and **b** the rate of photodissociation of H_2, as predicted by the "exact" numerical model (solid line) and by the FGK approximation (dashed line). **c** gives the ratio between the photodissociation rates calculated by the "exact" and the FGK model. All the data are relative to the "standard" model: $n = 20\ cm^{-3}$, $T = 80$ K

Figure 4a, b is the same as Fig. 3a, b for the first 4 rotational levels of H_2.

In Fig. 5 we show the influence of a higher density ($n = 100\ cm^{-3}$), and in Fig. 6 of a higher radiation field (multiplied by a factor of 5), on the abundances and the photodissociation rates. As expected, enhancing the photon flux shifts the transition region further in. On the other hand, a higher density provides a better shielding and the formation of H_2 is easier. At the edge of the cloud, H_2 molecules are destroyed rapidly by the radiation, so that the abundance is given by $[H_2] = k_G[H]^2/P_{phot}$, where P_{phot} is the photodissociation probability and k_G the rate of formation on grains. Since nearly all the hydrogen is in the form of H, this expression shows that, at the edge, the relative abundance of H_2 is proportional to the density.

Figure 7 shows the ratio of ortho to para H_2 in the transition region. A qualitative analysis can explain the very high value of this ratio at the transition. Let us consider a system of four species, H, H^+, H_2(o), H_2(p) (where o and p stand for ortho and

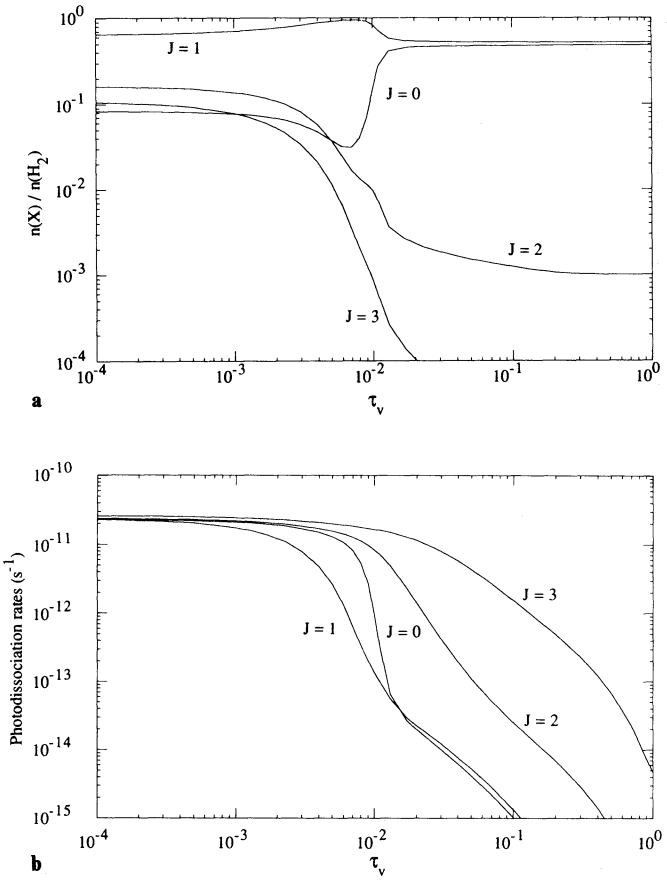

Fig. 4. **a** The relative populations of the rotational levels $0 \leq J \leq 3$ of H_2, and **b** the corresponding photodissociation rates

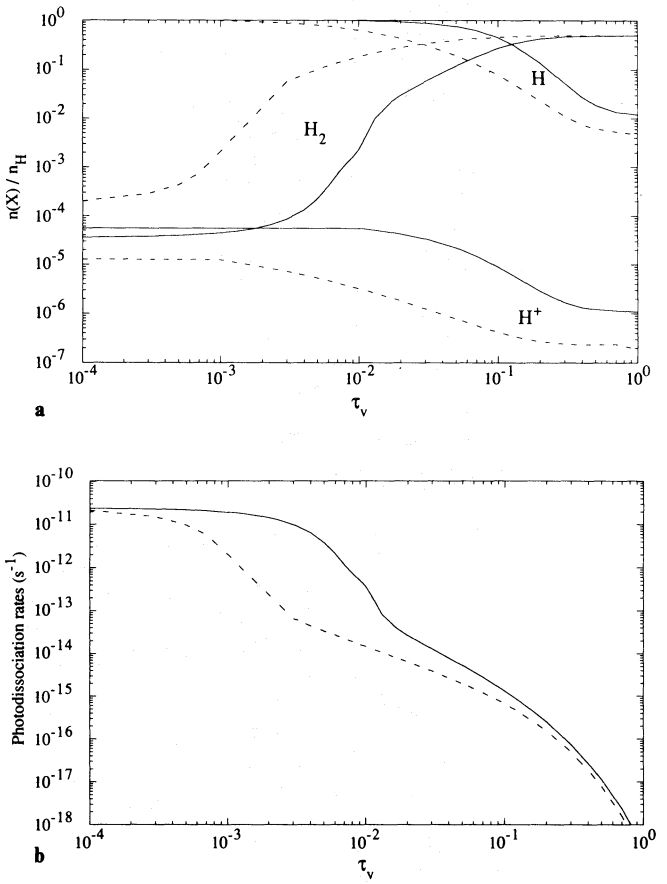

Fig. 5a and b. A comparison of **a** the relative abundance of H_2, H and H^+, and **b** the rate of photodissociation of H_2, for models in which $n_H = 20\ cm^{-3}$ (solid lines) and $n_H = 100\ cm^{-3}$ (dashed lines)

para), plus the grains (Gr), and of six reactions:

(1) $H + H + Gr \rightarrow H_2(p) + Gr$ rate: $k_G(cm^6\,s^{-1})$
(2) $H + H + Gr \rightarrow H_2(o) + Gr$ rate: $3k_G(cm^6\,s^{-1})$
(3) $H_2(p) + h\nu \rightarrow H + H$ rate: $P_p(s^{-1})$
(4) $H_2(o) + h\nu \rightarrow H + H$ rate: $P_o(s^{-1})$
(5) $H_2(p) + H^+ \rightarrow H_2(o) + H^+$ rate: $k_5(cm^3\,s^{-1})$
(6) $H_2(o) + H^+ \rightarrow H_2(p) + H^+$ rate: $k_6(cm^3\,s^{-1})$

Steady state implies that the creation of a molecule is exactly balanced by its destruction so that

$$\frac{d[H_2(p)]}{dt} = 0 \Rightarrow [H_2(p)] = \frac{k_G[H]^2 + k_6[H^+]\,[H_2(o)]}{P_p + k_5[H^+]},$$

$$\frac{d[H_2(o)]}{dt} = 0 \Rightarrow [H_2(o)] = \frac{3k_G[H]^2 + k_5[H^+]\,[H_2(o)]}{P_o + k_6[H^+]}.$$

This leads, after some rearrangement, to an ortho to para ratio of

$$\frac{[H_2(o)]}{[H_2(p)]} = \frac{3P_p + 4k_5[H^+]}{P_o + 4k_6[H^+]}.$$

Three cases deserve a comment.

(i) At the edge, H^+ is negligibly small and $P_o = P_p$. The resulting ortho to para ratio is determined from the assumptions made for the formation on grains, i.e. $[H_2(o)]/[H_2(p)] = 3$.

(ii) When shielding becomes effective, ortho H_2 is shielded slightly before para H_2 (see Fig. 4). As the variation is exponential, P_o becomes much smaller than P_p leading to the peak in Fig. 7.

(iii) When the conversion of H to H_2 is complete, both P_o and P_p are negligible as compared to proton exchange, and levels $J = 0$ and $J = 1$ of H_2 are thermalized. Then, $[H_2(J=1)]/[H_2(J=0)] = 9e^{-170.5/T} \approx 1$ at $T = 80$ K.

4. Validity of the equilibrium model

In common with similar studies of diffuse clouds, the calculations reported above refer to the static, equilibrium state of the gas, under the influence of an invariant extended radiation field. The equilibrium state is attained in the limit of $t \rightarrow \infty$. The model is realistic only if the main processes of formation and destruction of H_2 are sufficiently rapid compared to the timescale for the evolution (or formation) of the diffuse cloud.

In Fig. 8, we compare the principal rates (per unit volume) of formation and destruction of molecular hydrogen for a cloud with $T = 80$ K, $n_H = 20\ cm^{-3}$ and a standard radiation field (Rad = 1 is then defined as a multiplication factor of the energy density over the total range of wavelengths). At the outer edge of the cloud, H_2 is formed on grains and destroyed by photodissociation. As τ_v increases, destructive gas phase chemical processes become relatively more important until for $\tau_v \geq 0.3$, they dominate photodissociation as the main mechanism of destruction of H_2. Concerning the formation of H_2 through chemical

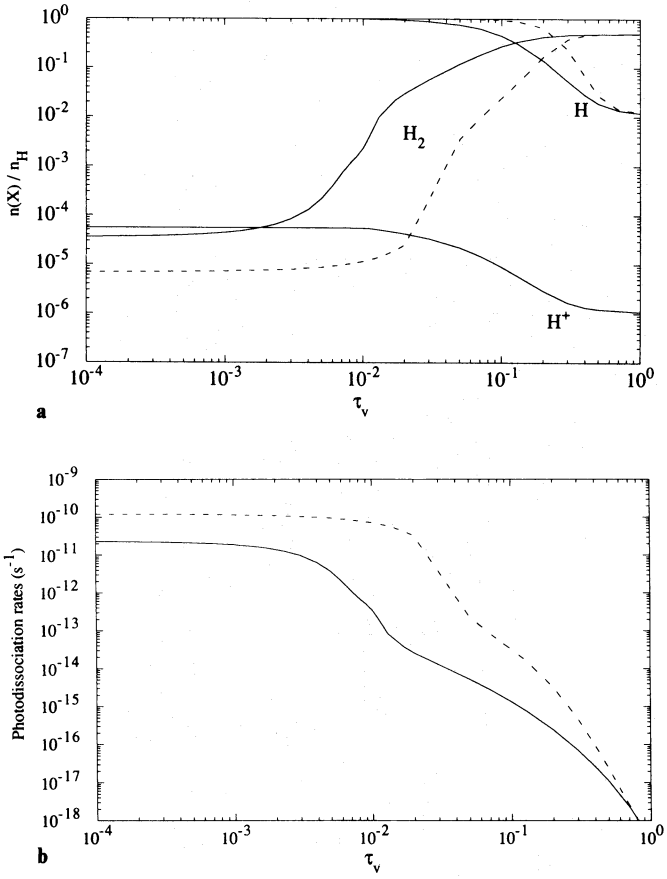

Fig. 6a and b. Same as Fig. 5, but comparing the results obtained with the standard interstellar radiation field (solid lines) and a field which is 5 times more intense at all wavelengths (dashed lines)

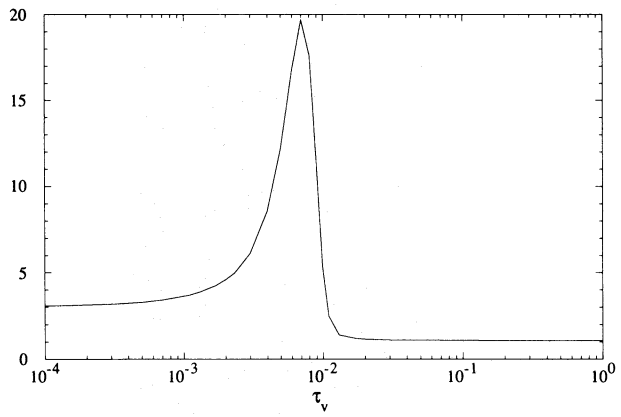

Fig. 7. The ortho:para H_2 density ratio, as predicted by the static equilibrium model

recycling, it mainly occurs at $\tau_v = 1$ through reactions involving the H_3^+ ion via electronic recombination and reactions with O and abundant species. Thus, the characteristic timescale for formation/destruction of H_2 is determined by photodissociation in the outer part of the H/H_2 transition region and by chemical processes in the inner part. This timescale is plotted in Fig. 9 for the three models considered in the present study.

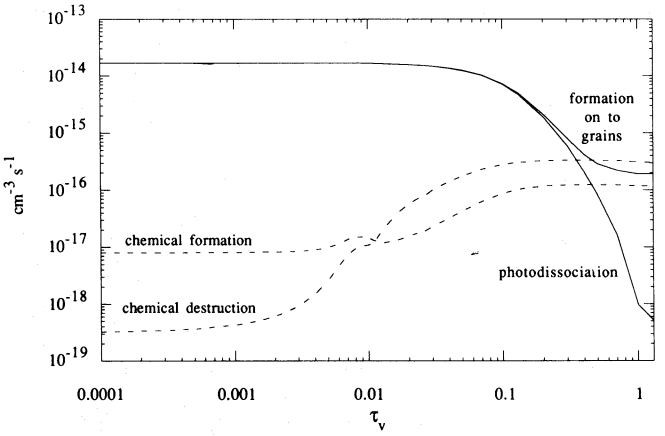

Fig. 8. Rates per unit volume of formation and destruction of H_2 on grains, through photodissociation or gas phase chemical reactions

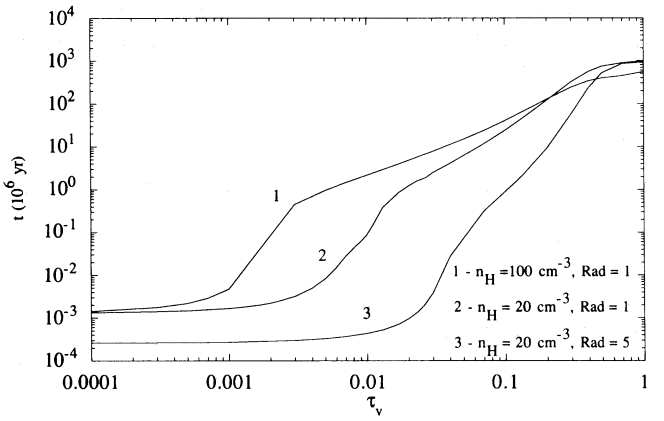

Fig. 9. The timescale characterizing the formation/destruction of H_2 for the three equilibrium models considered in the text

In the outer part of the cloud, the characteristic timescale increases as the incident intensity of the radiation field decreases or as the density n_H of the cloud rises, thereby increasing the degree of self-shielding. Deeper in the cloud, where gas phase chemical processes dominate, the timescales become comparable for all three models. However, their value, which approaches 10^9 yr, is clearly unrealistically large, compared to the probable cloud lifetimes. We conclude that the gas does not attain equilibrium towards the centres of diffuse clouds.

In order to investigate departures from equilibrium, we are currently adapting a time-dependent interstellar shock code developed by some of us (Heck et al. 1990). Initial results indicate that the time required to form H_2 in a model in which hydrogen is initially in atomic form is so large that less H_2 is present at early times than is indicated by the equilibrium model. However, unlike the equilibrium models presented above, the results of the time-dependent calculations depend on the initial composition that is assumed, and the solution is not unique. These factors will need careful consideration when comparing models with observations, a task that we reserve for a future publication.

5. Conclusions

We have made a detailed comparison of two different approaches, one approximate and one "exact", to solving the problem of

radiative transfer in molecular lines for a diffuse cloud in static equilibrium. The FGK approximation was found to be in good agreement with the exact results and is much less CPU time consuming. The availability of reliable J dependent photodissociation rates as well as discrete oscillator strengths of the Lyman and Werner bands of molecular hydrogen will enable us to consider the fluorescence excitation of H_2 in various static environments with fewer assumptions than in previous studies (Black & van Dishoeck 1987; Sternberg & Dalgarno 1989; Sternberg 1989). The photodissociation of H_2 (and CO) in interstellar shocks will also be studied, building on the earlier work of Monteiro et al. 1988.

The timescales of the formation and destruction mechanisms of H_2 have been analysed. The assumption of equilibrium has been examined and found to be of dubious validity when chemical gas phase reactions become of the same efficiency as photodissociation for destroying H_2.

Acknowledgement. This project received support from the GDR 0127 "Physico-Chimie des Molécules Interstellaires" of the CNRS and from the British Council.

References

Abgrall H., Launay F., Roueff E., Roncin J.-Y., 1987, J. Chem. Phys. 87, 2036
Abgrall H., Roueff E., 1989, A&AS 79, 313
Anders E., Grevesse N., 1989, Geochim. Cosmochim. Acta 53, 197
Black J.H., Dalgarno A., 1977, ApJS 34, 405
Black J.H., van Dishoeck E.F., 1987, ApJ 322, 412
Brown J.M., Hougen J.T., Huber K.P., Johns J.W.C., Kopp I., Lefebvre-Brion H., Merer A., Ramsay D.A., Rostas J., Zare R.N., 1975, Mol. Spectrosc. 55, 500
Dalgarno A., Herzberg G., Stephens T.L., 1970, ApJ 162, 49
Danby G., Flower D.R., Monteiro T.S., 1986, MNRAS 226, 739
Elitzur M., Watson W.D., 1978, A&A 70, 443
Federman S.R., Glassgold A.E., Kwan J., 1979, ApJ 277, 466
Ford A.L., 1975, J. Mol. Spectrosc. 56, 251
Gerlich D., 1990, J. Chem. Phys. 92, 2377
Heck L., Flower D.R., Pineau des Forêts G. 1990, Comp. Phys. Commun. 58, 169
Julienne P.S., 1973, J. Mol. Spectrosc. 48, 508
Le Bourlot J., 1991, A&A 242, 235
Martin C., Hurwitz M., Bowyer S., 1990, ApJ 354, 220
Mathis J.S., Metzger P.G., Panagia N., 1983, A&A 128, 212
Pineau des Forêts G., Flower D.R., Hartquist T.W., Dalgarno A., 1986, MNRAS 220, 801
Monteiro T.S., Flower D.R., Pineau des Forêts G., Roueff E., 1988, MNRAS 234, 863
Schmoranzer H., Noll T., Roueff E., Abgrall H., Bieneck R., 1990, Phys. Rev. A 42, 1835
Schofield K., 1967, Planet. Space Sci. 15, 643
Stecher T.P., Williams D.A., 1967, ApJL 149, 29
Stephens T.L., Dalgarno A., 1972, J. Quant. Spectrosc. Radiat. Transfer 12, 569
Sternberg A., Dalgarno A., 1989, ApJ 338, 197
Sternberg A., 1989, ApJ 347, 863
van Dishoeck E.F., 1988, in: Reactive Rate Coefficients in Astrochemistry. Millar T.J. Williams D.A. (eds.). Kluwer, Dordrecht, p. 73
van Dishoeck E.F., Black J. H., 1988, ApJ 334, 771
Viala Y.P., Roueff E., Abgrall H., 1988, A&A 190, 215